Progress In Electromagnetics Research C, Vol. 105, 129–146, 2020

Dual Band Circular Polarized Printed Dipole Antenna for S and C Band Wireless Applications

Gunaram[1], Jitendra K. Deegwal[2], and Vijay Sharma[3, *]

Abstract—In this article, a modified circular shape printed dipole structure is studied to achieve wide bandwidth and dual-band circular polarization (CP) behavior along with dual polarizations. The idea behind this structure is that asymmetric geometry can give rise to circular polarization with an optimized position of coaxial probe feed. The circular patches on both sides of the substrate are altered with elliptical slots at an optimized location in association with opening slots. With these alterations the impedance bandwidth for $S_{11} < -10$ dB is ranging from 2.36–7.34 GHz (4.98 GHz) which is nearly 102.5% about mid-point frequency 4.85 GHz. The antenna resonates at a lower band (1.55 GHz) and shows linear polarization (LP) operation at that band whereas dual CP bands with dual senses are obtained at higher frequency ranges 4.00–4.60 GHz and 6.07–7.13 GHz respectively with 3-dB axial ratio bandwidth of 13.7% and 16.6%. The simulated and measured experimental results are in close agreement. This antenna is suitable to be used for navigation purposes, radar communication, and wireless communication (especially wireless avionics intra communications) in S and C bands, respectively.

1. INTRODUCTION

For a linearly polarized antenna, if the transmitter and receiver antennas are placed orthogonal to each other the received signal strength will be very weak, and it will be strong only if both the antennas (transmitter and receiver) are aligned properly. In many communication system applications, it becomes quite difficult to manage the alignment or orientation of the antenna. To overcome this issue, the circularly polarized (CP) antenna is promising, because in this category of antenna the received signal strength is independent of the orientation of transmitter and receiver antennas [1]. Nowadays circularly polarized (CP) antennas attain more focus due to the fast growth of wireless communication systems. Modern days communication systems work for multiple frequencies simultaneously thus require wide bandwidth. These systems can use single-band CP antennas through different employed frequencies to come across the requirements of multi-systems. However, to adjust these requirements in communication systems, issues like large size/volume in turn increase the cost of the antenna [2].

A conventional single-feed microstrip CP antenna has narrow 3-dB axial ratio bandwidth (ARBW) (less than 2%); however, high impedance bandwidth (IBW) can be achieved by altering the geometry. But in most of the cases, alteration in conventional geometry cannot guarantee a high ARBW. Researchers working in the antenna field have discovered new ways and techniques to overcome this issue, without affecting other parameters. A summary of efforts and focus devoted to this issue by scientists and researchers in current time is as follows. In [3], an assembly of elliptical shape gap coupled patches is presented by Sharma et al. to achieve the CP with wide bandwidth and suitable radiation performance;

Received 3 May 2020, Accepted 28 August 2020, Scheduled 14 September 2020

* Corresponding author: Vijay Sharma (phyvijay@gmail.com).

[1] Department of Physics, Bhagwant University, Ajmer, Rajasthan, India. [2] Department of Electrical Engineering, Govt. Mahila Engineering College, Ajmer, Rajasthan, India. [3] Department of Physics, Govt. Mahila Engineering College, Ajmer, Rajasthan, India.

however, in this arrangement the size on the antenna is an issue, which limits its use. In [4], a dual-band stacked single-feed CP antenna is presented by Kumar et al., which gives ARBWs 1.3% and 1.1% for upper and lower bands respectively with a very small frequency ratio of 1.03. However, due to stacking, the volume of antenna increases which becomes a constraint in some applications. In [5], a planar monopole antenna for dual-band CP behaviour is presented by Tan and Wang, which has two strips. One is of L-shape and other of C-shape for the lower band (2.32–2.70 GHz) and upper band (4.76–6 GHz) respectively with ARBWs of 180 MHz and 870 MHz in the broadside direction. In [6], a planar modified L-shaped monopole having altered ground and inverted-L strip (responsible for CP and dual-band) is presented by Li et al. The gain of the offered antenna is found low due to FR4 substrate which can be improved with the replacement of high-grade material. For radio frequency identification (RFID) application, Kumar et al. [7] present a square patch on which three slots (one rectangular shape and two triangular shapes) along the diagonal are etched. The orientation and dimension of slots are optimized to achieve CP radiations. The offered antenna resonates at low-frequency 0.91 GHz at a cost of large volume size which is $80 \times 80 \times 4.572\,\text{mm}^3$. This size of the antenna can be reduced by applying size reduction techniques which include meandering in the ground plane and/or in the patch. In [8] by Maddio et al., with the combination of gap-coupled concept and arc-shaped slits in a circular patch, a dual-band CP antenna is achieved at frequencies 2.45 GHz and 5.10 GHz applicable in Wi-Fi operation. Circular polarization is observed due to the overlapping of TM_{11} and TM_{12} modes. In [9], to produce CP with dual-frequency Bao and Ammann present a circular patch antenna encircled by a couple of annular-rings and having a cross-slot of unequal length in ground. By optimizing the dimension of the circular patch and annular-rings, the small frequency ratio can be tuned. Wang et al. [10] present an aperture-shared dual-polarized (CP in S-band and LP in X-band) patch antenna with the use of stacked and parasitic patches. High port isolation of 32 dB between these two bands (S-band and X-band) is achieved with the offered antenna.

In [11], the performance of a monofilar spiral slot antenna for dual frequencies and CP behaviour is reported by Bao and Ammann. It is found that dual CP senses are observed because of the rotation of current in two opposite directions. In [12], Kandasamy et al. apply split-ring resonators (SRRs) in a corner truncated square slot antenna to achieve CP performance. The theoretical analysis of antenna is also discussed which explains that resonance frequencies and polarization sense in both the bands can be accomplished individually. In [13], Bhattacharjee et al. offer a miniature wearable antenna capable of operating in the ISM band with a linearly polarized (LP) pattern at 2.45 GHz and circularly polarized (CP) pattern at 5.8 GHz. The resonance modes of the ground plane are computed with the help of a characteristic mode analysis (CMA) technique. In [14], a dual-band dual-sense CP antenna with rotational symmetry of dipole structure is reported by Xu et al., which is upgraded from a bow-tie dipole antenna (linear polarized). In [15], a compact planar inverted F-Antenna is presented by Bhattacharjee et al. for dual-band (ISM 2.45 GHz band and 4G long term evolution band) and dual-polarized operation. To grasp the antenna performance in ON body conditions, a single and multi-layer tissue model is applied, and minimal deviations from the free space environment are attained which reflects that for body-centric communications porotype is a possible candidate. Recently, Midya et al. [16] propose a dual-band dual-polarized antenna which consists of a rotated U-shaped patch and a slanting-edge ground plane. This design gives an ARBW of 73.54% (3.80–8.22 GHz) and bandwidth of 29.84% (1.54–2.08 GHz) for linearly polarized radiation. The literature addressed here shows that wide-band and dual-band antenna with circular polarization is a sizzling research topic in current time. However, not much attention is paid to achieve a CP antenna with dual bands, dual senses, and a dipole structure.

In this article, the design of a wide-band dual-polarized CP antenna is presented to encounter the necessities of communication systems in one module. The dual senses and dual CP bands are achieved by etching elliptical slots of appropriate dimension in-ground and patch at a suitable place in association with an opening slot. The offered antenna has been fabricated after multiple computer simulations and examined experimentally. The design analysis of antenna configuration with a parametric study of the different parameters is also undertaken. The experimental results and comprehensive outcomes of the present study are discussed in further sections.

2. EVOLUTION PROCEDURE OF ANTENNA SCHEMATIC

Three designs are outlined, to validate the improvement strategy, as shown in Figs. 1(a)–(c). Antenna 1 is a conventional circular patch microstrip antenna (CPMA) printed on an FR-4 substrate along with a microstrip line in the same plane. This is backed by another printed circular patch on the other side acting as a ground. This antenna is fed by a coaxial probe via ground, which is connected with the microstrip line as depicts in Fig. 1(a). The characteristics curve that describes the behaviour of antenna in terms of impedance bandwidth (IBW), gain, and the presence of circular polarization (CP) for antennas 1, 2, and 3 is described in this section. From Fig. 2, it is observed that antenna 1 gives the first resonance at 2.19 GHz, and the two higher-order resonances are at 6.32 GHz and 8.34 GHz. All three resonances are superimposing each other and resulting in a wider IBW nearly 121% (1.85–7.54 GHz) about the mid-frequency 4.69 GHz. Also there exist two humps (close to −10 dB level) at frequencies 3.0 GHz and 7.5 GHz, respectively.

The theoretical lower band-edge frequency corresponds to −10 dB, and S_{11} is 1.97 GHz, calculated

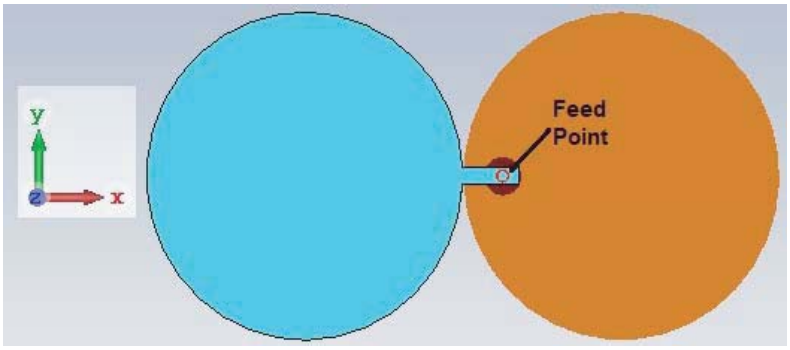

(a)

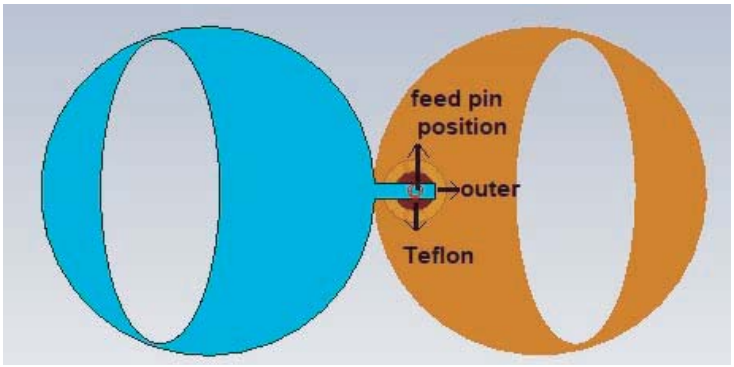

(b)

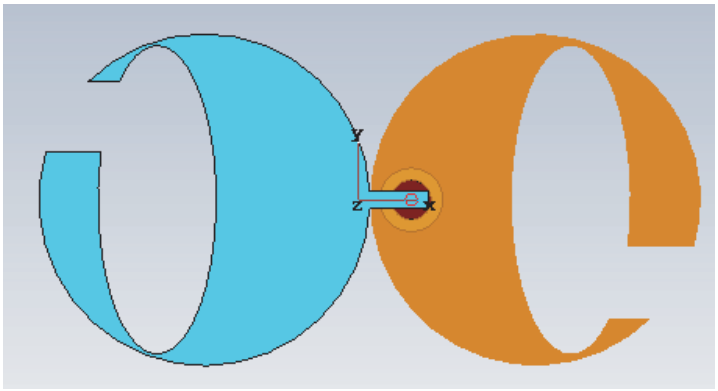

(c)

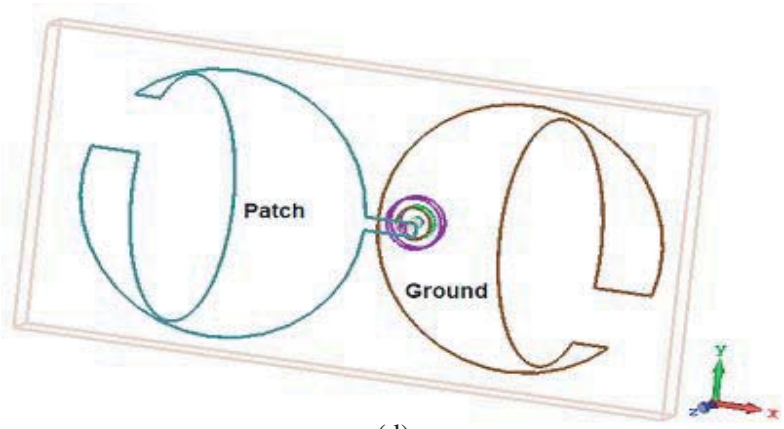

(d)

Figure 1. Progress of final design. (a) Antenna 1, (b) Antenna 2 and (c) Antenna 3, (d) view of feed system for 'Antenna 3'.

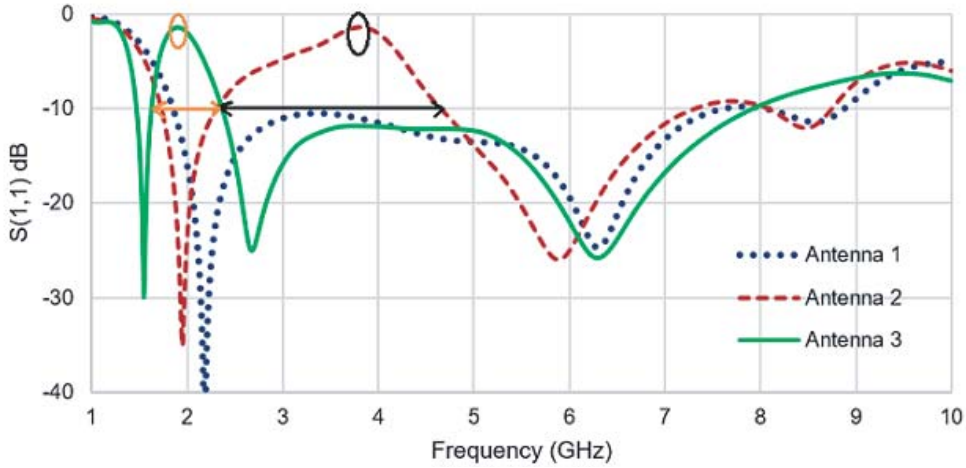

Figure 2. Variation of $S(1,1)$ in dB with frequency for (a) Antenna 1, (b) Antenna 2, and (c) Antenna 3.

using the expression [17]:

$$f_l = \frac{c}{\lambda} = \frac{7.2}{(L + r + p)}\,\text{GHz} \tag{1}$$

which is close to computed frequency 1.85 GHz. Here $L = 2R$ and $r = \frac{R}{4}$, R is the radius of circular radiator patch and p the feed gap (in cm).

Also, antenna 1 exhibits linear polarization (LP) as the axial ratio (AR) value is very large (above 6 dB) for the entire frequency range of interest as presented in Fig. 3.

To further improve antenna 1 (Fig. 1(a)), in terms of IBW and CP, it has to be modified by loading some cuts/slots to alter the surface current distribution on metallic patch and ground. Two elliptical slots (one in the ground and the other in the patch) are loaded for this purpose in antenna 1 as shown in Fig. 1(b) and named this as antenna 2. The S_{11} variation for antenna 2 with frequency is depicted in Fig. 2, which reflects that it is now resonating as a dual-band and for first band resonance frequency is $f_1 = 1.95$ GHz (2.98%) and for second band resonance frequency is $f_2 = 5.88$ GHz (44.57%). Instead of large IBW, this dual-mode is observed, and it is likely because the resonant mode created by these elliptical slots does not overlap with the fundamental resonant mode of the circular patch with the existing arrangement. The elliptical slot of the optimized dimension acts as a band rejection element at nearly 3.88 GHz. A reduction in frequency for all the three resonances is also observed due to lengthening

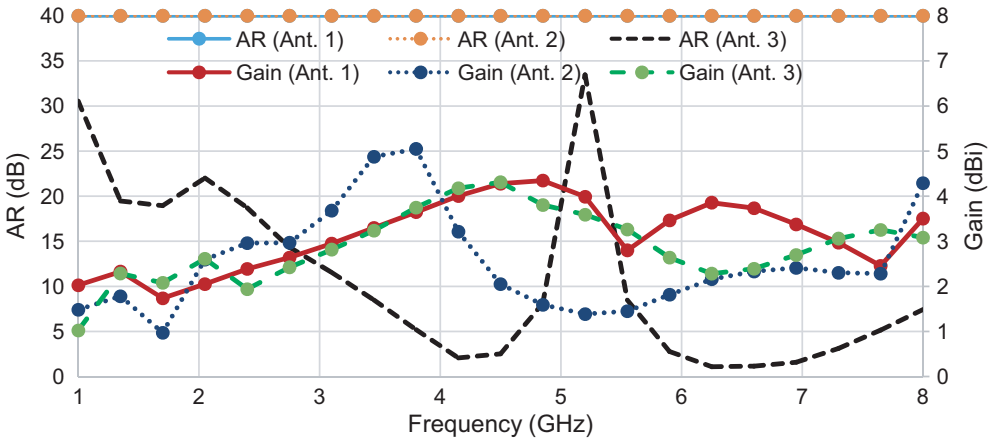

Figure 3. Variation of AR (in dB) and Gain (in dBi) with frequency for (a) Antenna 1, (b) Antenna 2, and (c) Antenna 3.

of the current path. Wideband is still there for the higher band, with a rejection band. However, in this case, the current density increase on the periphery of these elliptical slots and a rotation of field are detected, but the component is not orthogonal with the time phase. The AR value is still very high (above 6 dB) as shown in Fig. 3, which exhibits that the antenna is still linearly polarized for both the bands.

Keeping this in mind to generate an orthogonal vector of equal amplitude to generate CP the design of antenna 2 is further amended by opening the elliptical slots etched in circular patch and ground. The dimension and position of opening slots are optimized, and the final geometry 'antenna 3' is attained as presented in Fig. 1(c). A glass epoxy FR4 substrate is used for the design of antenna having parameters value $\varepsilon_r = 4.4$, $\tan\delta = 0.025$. The overall volume of this antenna is $64 \times 32 \times 1.59\,\text{mm}^3$. In this design, the left side portion of the dipole antenna is printed on the upper surface of the substrate (act as a patch) whereas the right side portion of the dipole is printed on the lower surface (acts as a ground). To maintain the rotational symmetry, the dipole is made up of two circular patches of the same radius 'R' at coordinate $(-R, 0)$, and the feeding point is fixed at $(F_d, 0)$. To attain dual-band CP radiation, a couple of elliptical slots of dimensions $a_1 \times b_1$ and $a_2 \times b_2$ are etched in the ground as well as patch. A wide gap of optimum dimension is also introduced at the circumference of circular shape ground and patch such that the elliptical slot becomes open.

To energize the patch, a feed line of optimum dimension $(L_f \times W_f)$ is connected to the upper circular patch, which is fed by an SMA connector via lower circular ground. The innermost pin is attached to the feed line, which is in direct contact of the patch via ground, whereas the exterior part of the SMA connector is in contact with the ground plane and insulated from the metal pin with Teflon coating on a metal pin. The final layout with geometrical parameters is shown in Fig. 4. Feed System for antennas 1, 2, and 3 are the same. To show the feeding system more clearly, the wire diagram of the final design is given in Fig. 1(d). To assess the performance of the proposed antenna, CST Microwave Studio v.17 is used [18]. A large number of the simulations are brought out to optimize the design parameters, and final values of these parameters are recorded in Table 1.

It is observed from Fig. 2 that in the case of 'antenna 3' the two higher-order resonances come closer and gives rise to a wide simulated IBW 2.36–7.86 GHz (107%) about mid-frequency 5.12 GHz corresponding to −10 dB points on S_{11} curve; however, the fundamental mode appears as isolated at 1.55 GHz, and it is not combined with these two higher modes. Also, the hump becomes narrower in this case than the case for antenna 2, resulting in a wide bandwidth. From Fig. 3, it is perceived that AR value for both the antennas 1 and 2 is close to 40 dB, which corresponds to 0% 3 dB ARBW bandwidth. However, with the insertion of these two wide slots, AR value (in dB) is significantly reduced and gives rise to 3 dB ARBW in two bands. In the first band, the simulated ARBW is nearly 11.5% for frequency range 4.04–4.53 GHz (4.28 GHz) whereas in the second band, it is 20.9% for frequency range 5.89–7.27 GHz (6.58 GHz) as depicted in Fig. 3.

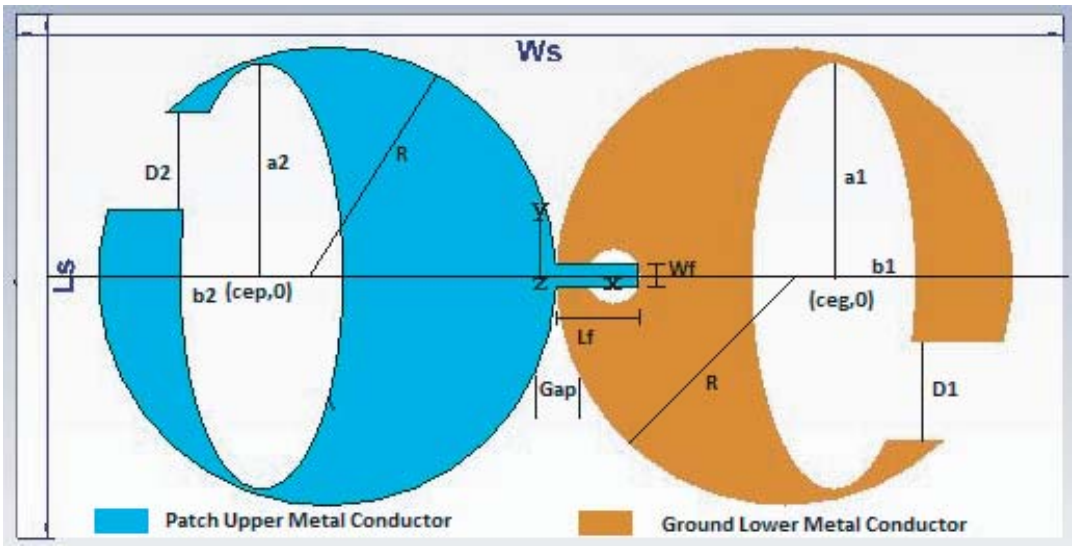

Figure 4. Top view of the proposed antenna geometry.

Table 1. Typical geometrical parameters of proposed antenna.

Parameter	Dimension (Unit: mm)
Radius of circular radiator patch/ground (R)	14.0
Dimension of semi major axis of elliptical slot ($a_1 = a_2$)	13.0
Dimension of semi minor axis of elliptical slot ($b_1 = b_2$)	5.0
Coordinate of elliptical slot in ground (ceg)	18.0
Coordinate of elliptical slot in Patch (cep)	17.0
Opening slot in patch (D_1)	6.0
Opening slot in ground (D_2)	6.0
Gap (g)	0.0
Feed strip (length) (L_f)	5.0
Feed strip (width) 'W_f'	1.4
Position of feed point along x-axis 'x_f'	4.5
Length of the substrate material (L_s)	32.0
Length of the substrate material (W_s)	64.0

3. ANALYSIS OF CP MECHANISM

To generate the CP radiation, it is essential to produce a component of the electric field with a phase variation of 90 degrees and identical amplitudes. Keeping this fact in mind, a further attempt is made to increase the current path lengths in antenna 2 (with some more alteration in configuration). To realize this, two wide slots are introduced on the periphery of circular patch and ground, respectively, such that it makes open the elliptical slots loaded in antenna 2 as shown in Fig. 1(c). The position and width of these wide slots in patch and ground are the key factors for the generation of the CP radiation. This not only gives a wide 3 dB ARBW but also maintains the IBW value.

To realize the CP mechanism, the illustrations of surface current distributions for 'antenna 3' at different instants of time ($t = 0$, $t = T/4$, $t = T/2$, and $t = 3T/4$) are given in Fig. 5 and Fig. 6, respectively. In the first 3 dB axial ratio band (4.0–4.6 GHz), the surface current vectors rotation is

analysed at 4.28 GHz. From Figs. 5(a)–(d), it can be observed that the majority of the surface current vectors, on the patch and ground plane, rotate in the clockwise direction, hence it improves the radiation in the same direction. Figs. 5(a)–(d) illustrate that 'antenna 3' radiates left-handed circularly polarized (LHCP) wave at the frequency 4.28 GHz [19].

In the second 3 dB axial ratio frequency band (6.04–7.13 GHz), the rotation of the surface current

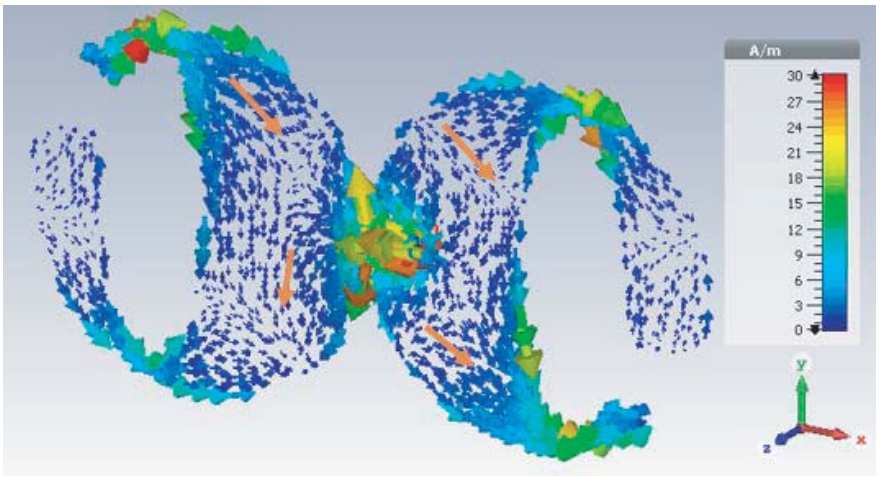

(a)

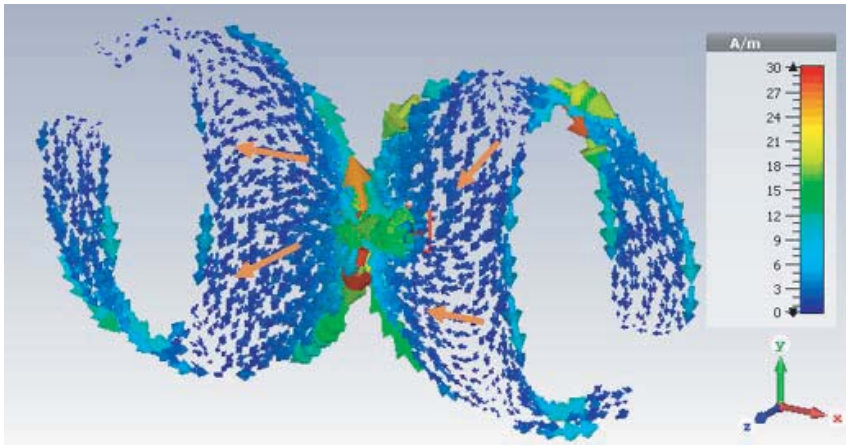

(b)

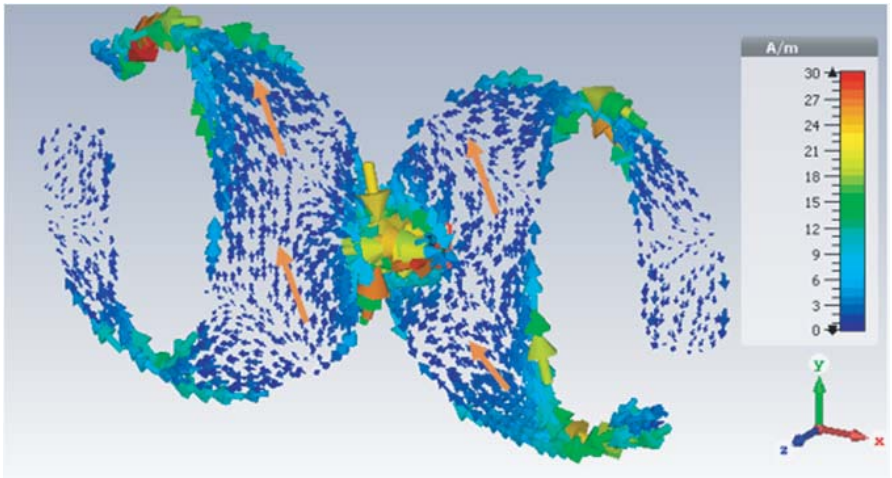

(c)

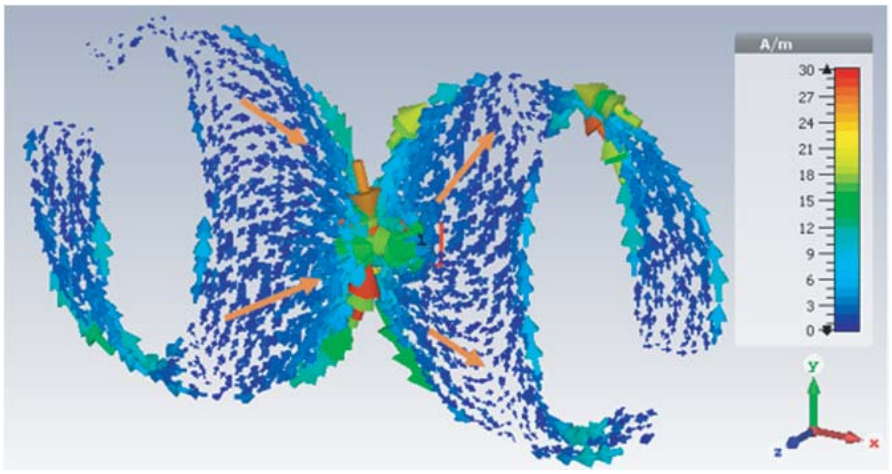

(d)

Figure 5. (a) The distributions of surface current simulated at 4.28 GHz for $t = 0$ ($\Phi = 0°$). (b) The distributions of surface current simulated at 4.28 GHz for $t = T/4$ ($\Phi = 90°$). (c) The distributions of surface current simulated at 4.28 GHz for $t = T/2$ ($\Phi = 180°$). (d) The distributions of surface current simulated at 4.28 GHz for $t = 3T/4$ ($\Phi = 270°$).

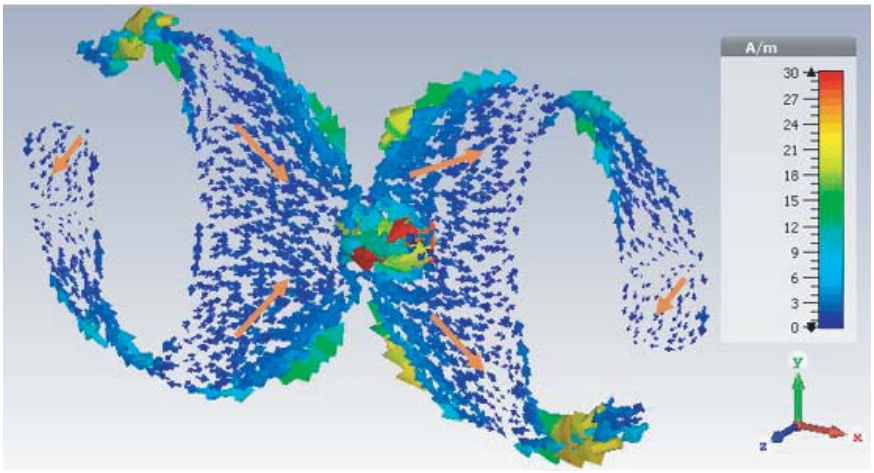

(a)

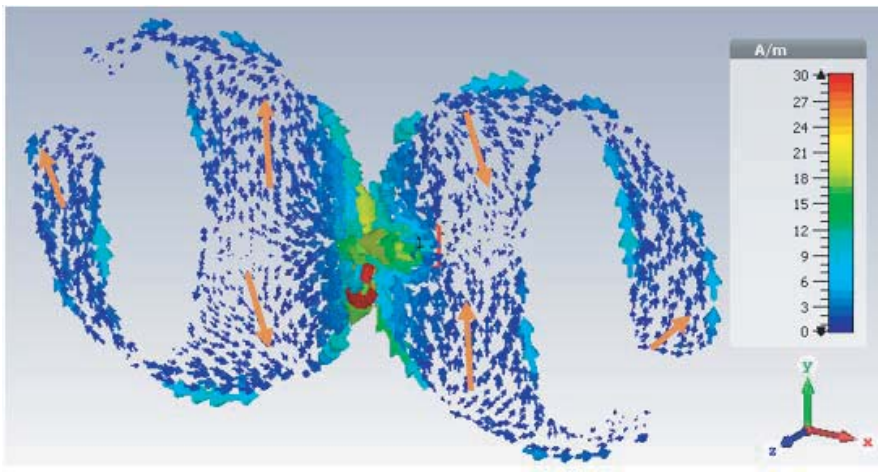

(b)

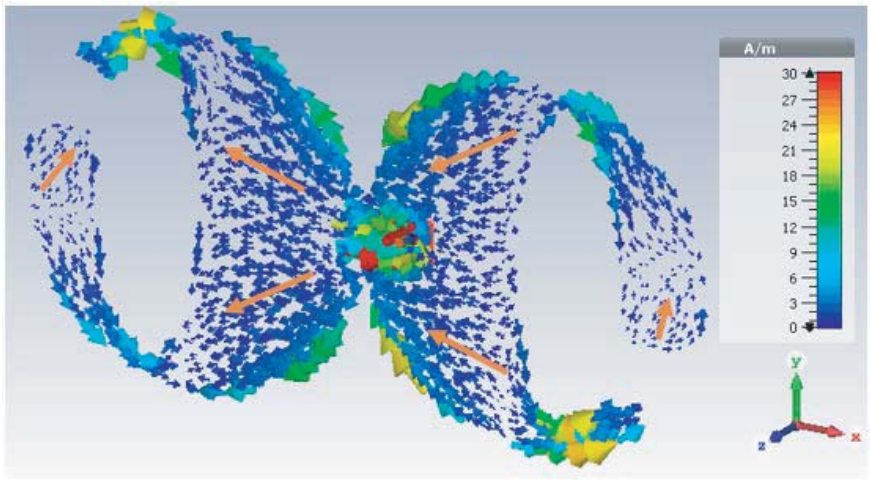

(c)

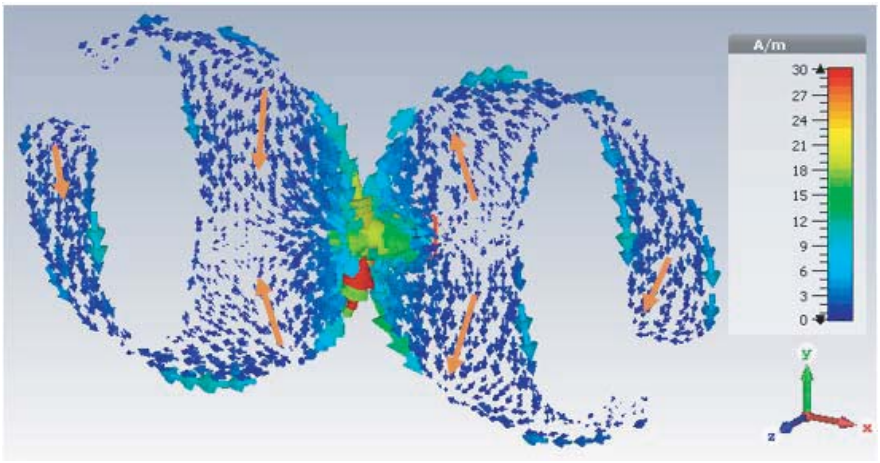

(d)

Figure 6. (a) The distributions of surface current simulated at 6.3 GHz for $t = 0$ ($\Phi = 0°$). (b) The distributions of surface current simulated at 6.3 GHz for $t = T/4$ ($\Phi = 90°$). (c) The distributions of surface current simulated at 6.3 GHz for $t = T/2$ ($\Phi = 180°$). (d) The distributions of surface current simulated at 6.3 GHz for $t = 3T/4$ ($\Phi = 270°$).

vectors is analysed at 6.30 GHz as shown in Figs. 6(a)–(d). It is perceived that the densities of the current vectors are almost the same on the wider area of the patch and the ground plane. It is also observed from Figs. 6(a)–(d) that half of the surface current vectors (upper half vectors) on the patch rotate in the anticlockwise direction, and remaining half current vectors (lower half) rotate in the clockwise direction, due to which the overall radiation from the wider area is linearly polarized. Perhaps the current vectors rotating on the long arm of the patch ellipse are in clockwise. Similarly, on the wider surface area of the ground plane, the current vectors cancel out each other's effect. However, the current vectors rotating on the long arm of the ground plane are in the anticlockwise direction that makes the radiation right-hand circularly polarized (RHCP) [20].

4. OPTIMIZATION OF VARIOUS PARAMETERS

To explore the consequences of essential parameters on antenna performance includes S_{11} and AR, and the parametric study has been accomplished in this section. The simulated S_{11} and AR plots for different values of parameters such as (i) variation in the width of opening slot 'D1' in the ground and 'D2' in the patch, (ii) the gap between the outer boundary (circumference) of the circular patch and

ground, and (iii) the feed point location along the x-axis are discussed to understand the effect of these parameters on S_{11} and AR. The substrate size and dimension of circular patch and ground are kept fixed.

4.1. Variation in Width of Opening Slot 'D1' in Ground and 'D2' in Patch

The variation in the width of the opening slot 'D1' in the ground and 'D2' in patch plays the most significant role in analysing the S_{11} and AR of the presented antenna design. Here one end of the slot along the Y-axis is kept fixed, and the second end is moved from origin to another end so that the slot width can be reduced as desired.

Figures 7–10 show that no significant change in the variation of S_{11} with frequency is observed with the change in slot width for higher frequencies; however, it affects the first resonance reasonably. A clear effect on ARBW and AR value is also observed. As the value of D1 or D2 decreases, the AR value also decreases. When there is no passage ($D1 = D2 = 0.0$ mm), this antenna 3 transforms into antenna 2, which gives no ARBW (as shown in Fig. 3). It is also observed that with increasing the value of D1 or D2 no effect on the first band of ARBW is observed; however in the second band, ARBW shifts towards higher frequency side. Again a lot of effort is given to optimize the final values as $D1 = D2 = 6.0$ mm.

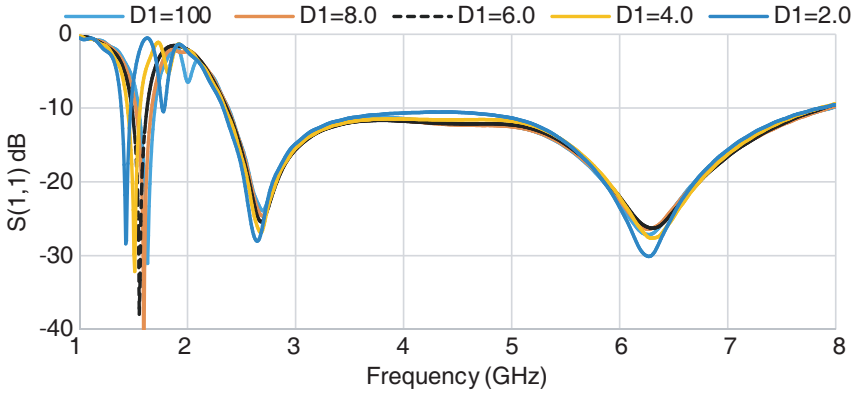

Figure 7. Effects of various D1 on S_{11}.

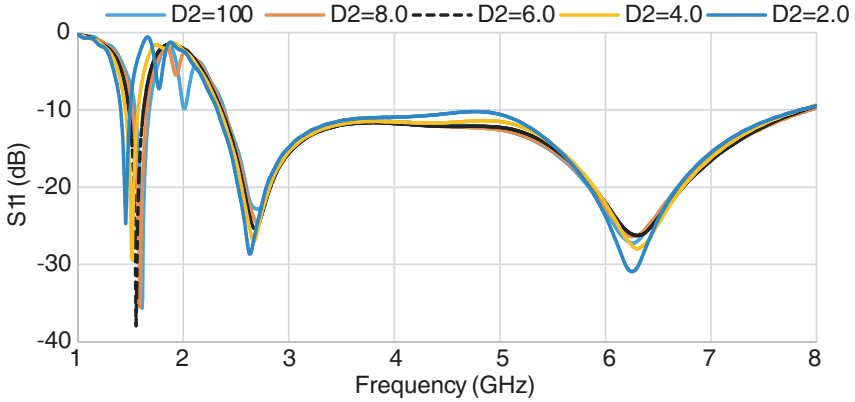

Figure 8. Effects of various D2 on S_{11}.

4.2. Effect of Gap between Patch and Ground 'g'

One of the major factors that controls the S_{11} and AR is the gap between patch and ground 'g'. It is observed from Figs. 11–12 that for large gap value IBW improves; however, the ARBW decreases in

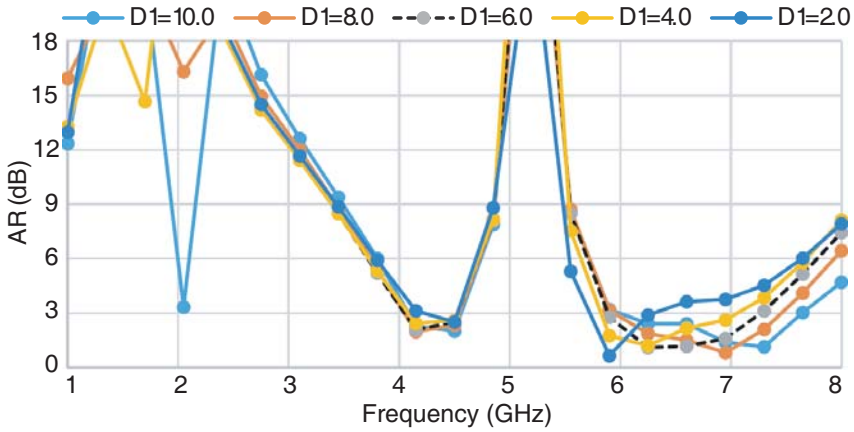

Figure 9. Effects of various D1 on AR.

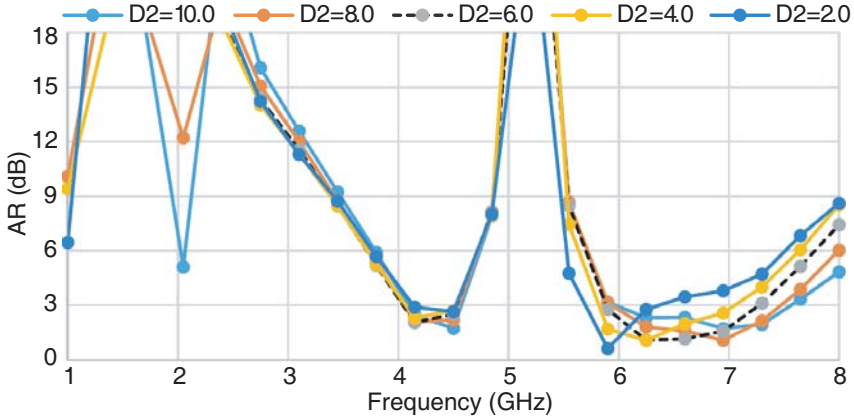

Figure 10. Effects of various D2 on AR.

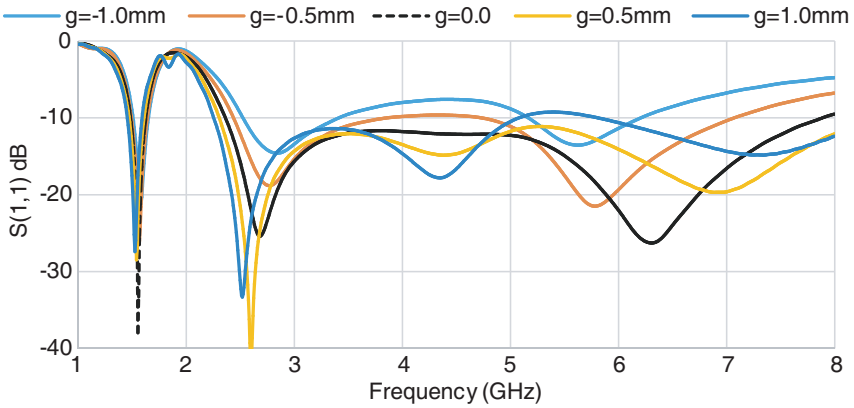

Figure 11. Variation of scattering parameter $S(1,1)$ with frequency for different gap value 'g'.

the higher band. On the other hand, if a slight portion of both the geometries (modified circular patch and ground) overlaps, it decreases the IBW but gives a good ARBW with a very low value of AR. So again an optimized value of gap 'g' is chosen, for the final antenna design. The value of g is taken zero, which means that the patch and ground are nearby without overlapping in two different planes.

4.3. Variation of Feed Point 'xf'

The effect of changing the feed point 'xf' on S_{11} and AR is depicted in Figs. 13–14. It is perceived that there is no effect on AR with this change. However, it affects S_{11} considerably. By proper positioning of the feed point, the IBW can be controlled or tuned for a certain range. The final value for the feed point is taken (4.5 mm, 0).

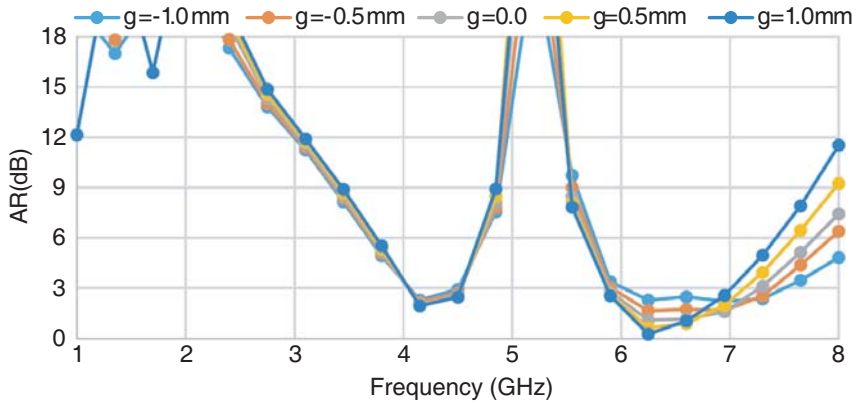

Figure 12. Variation in AR value with frequency for different gap value 'g'.

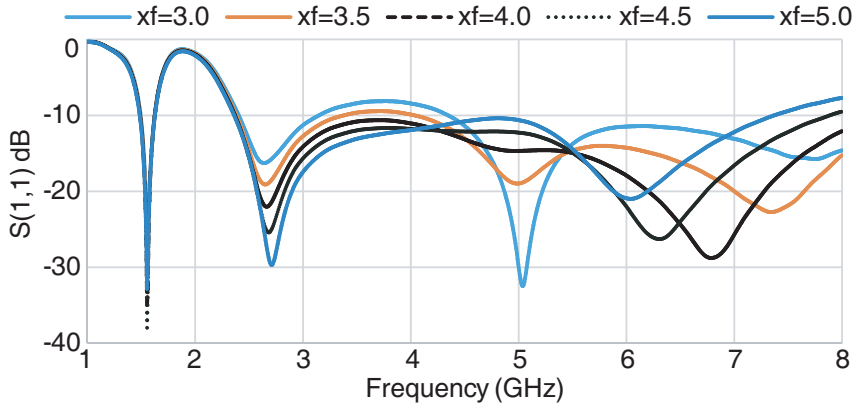

Figure 13. Variation of scattering parameter $S(1,1)$ with frequency for different feed point 'xf'.

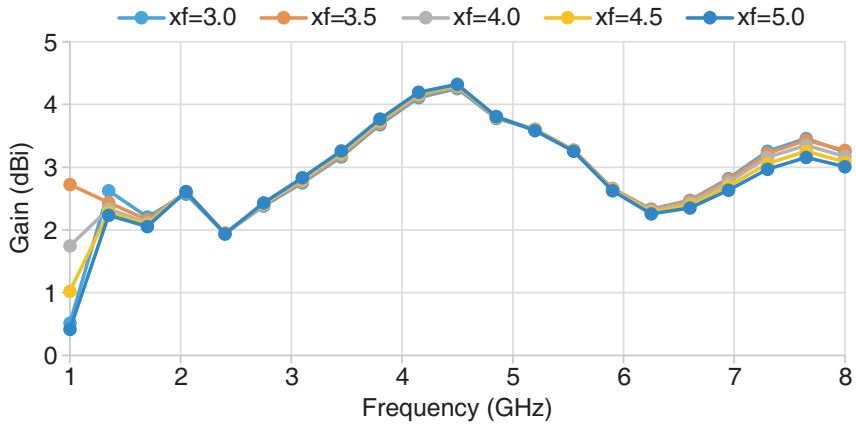

Figure 14. Variation in AR value with frequency for different feed point 'xf'.

5. EXPERIMENTAL RESULTS AND DISCUSSION

The design of the prototype antenna presented here is fabricated on an FR-4 substrate to confirm the design reliability. Photographs of the fabricated antenna front side (in an anechoic chamber) for radiation pattern measurement and back is shown in Figs. 15(a)–(b). The comparison of the simulated and measured S-parameter is elaborated to validate the results as given in Fig. 16. The simulated S-parameter is established by utilizing full-wave CST MWS whereas the Agilent N5234A PNA-L vector network analyser (VNA) [21] is used for the S-parameter measurement. It is replicated from Fig. 16 that measured resonance is at 2.72 GHz and 6.07 GHz with −10 dB impedance bandwidth ranging 2.36–7.34 GHz (102.5%), whereas the simulated resonance is at 2.63 GHz and 6.32 GHz with −10 dB impedance bandwidth 2.36–7.86 GHz (107%). It is perceived that there is a slight deviation in measured and simulated S_{11} variation with frequency, which is probably due to divergence in business accessible dielectric material properties or applied boundary conditions.

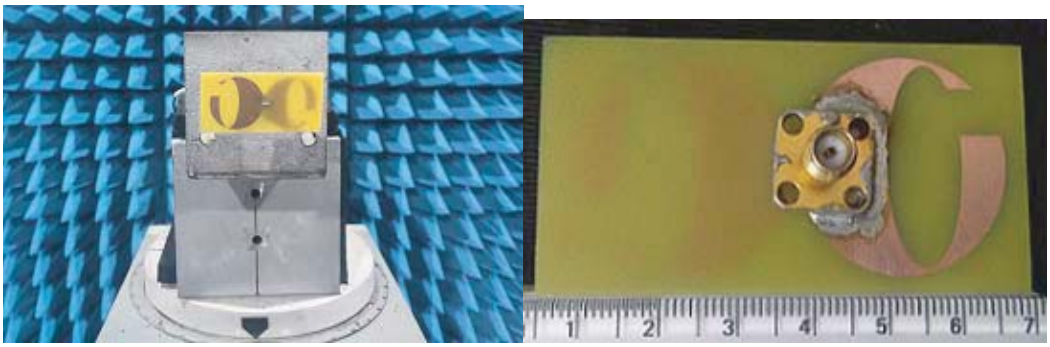

(a) (b)

Figure 15. Photograph of the fabricated antenna. (a) Front side (in anechoic chamber) and (b) back side.

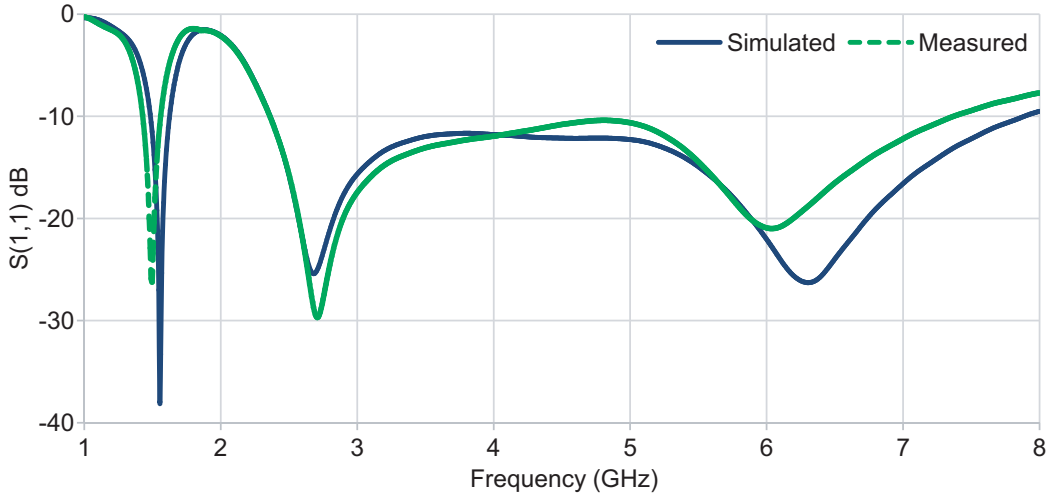

Figure 16. The measured S_{11} parameter for proposed antenna geometry.

Co- and cross-polarization patterns (simulated and measured) for final design 'antenna 3' at frequency 1.55 GHz, where linear polarization is achieved, are displayed in Figs. 17(a)–(b). An anechoic chamber is used for the measurement of the radiation pattern. The radiation pattern in the H-plane for co-polarization is omnidirectional, whereas the radiation pattern in the E-plane is more directional than that in the H-plane. It is also found that cross-polarization is more than 20 dB below in comparison to

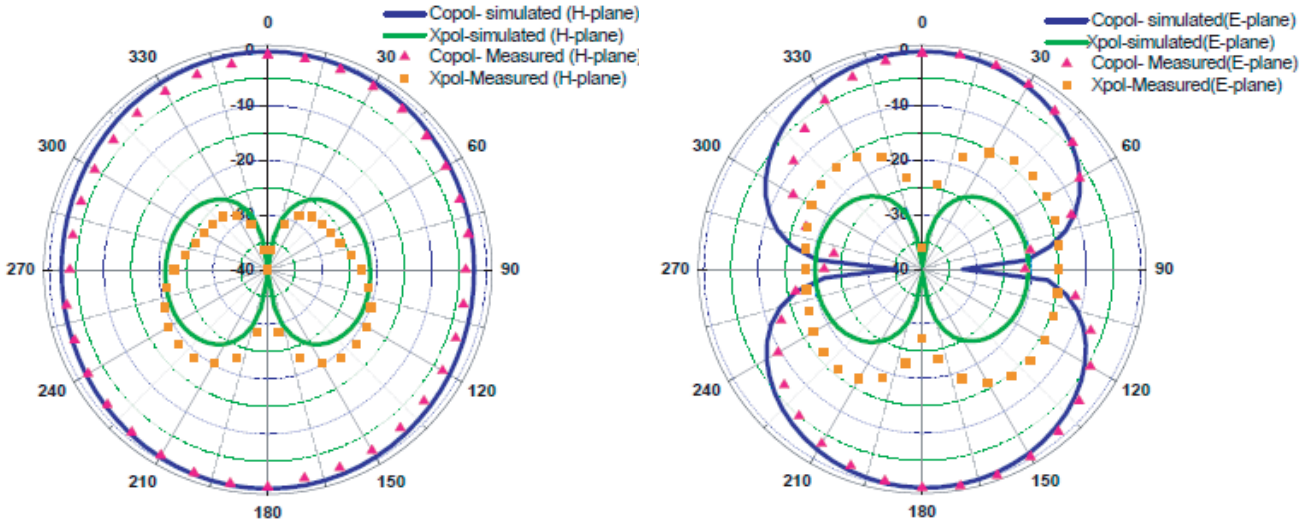

Figure 17. Normalized radiation patterns at 1.55 GHz. (a) XZ plane. (b) YZ plane.

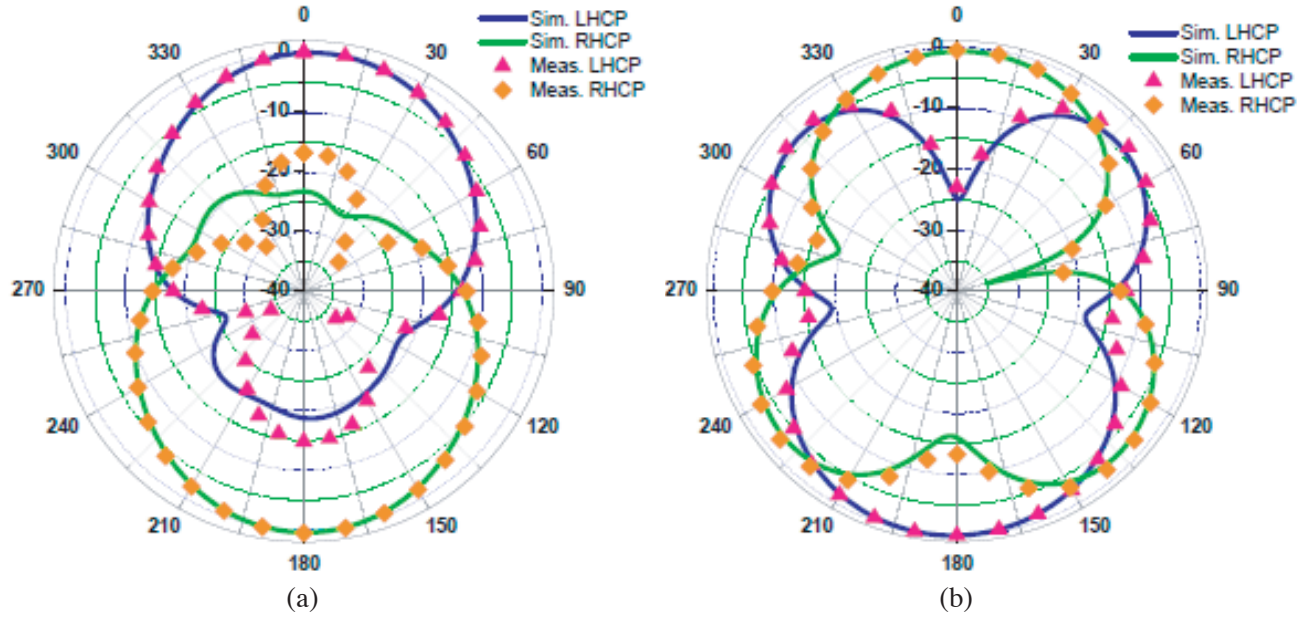

Figure 18. The numerical and measured CP radiation patterns (LHCP and RHCP) at (a) 4.28 GHz and (b) 6.3 GHz in XZ plane.

the co-polarization level in both the planes.

The numerical and measured CP radiation patterns at (a) 4.28 GHz and (b) 6.3 GHz in the XZ plane and YZ plane are displayed in Figs. 18(a)–(b) and Figs. 19(a)–(b). The measurements of LHCP and RHCP of the antenna are performed by the phase-amplitude method as this gives all the data required for complete polarization determination [22]. It is shown that the cross-polar levels are nearly 16 dB down in the direction of the main beam. The antenna radiates a bidirectional wave with opposite sense circular polarization. There is acceptable agreement between the measured and simulated results, and the observed small discrepancies between the measured and simulated results may probably be caused by fabrication imperfection and cable effects.

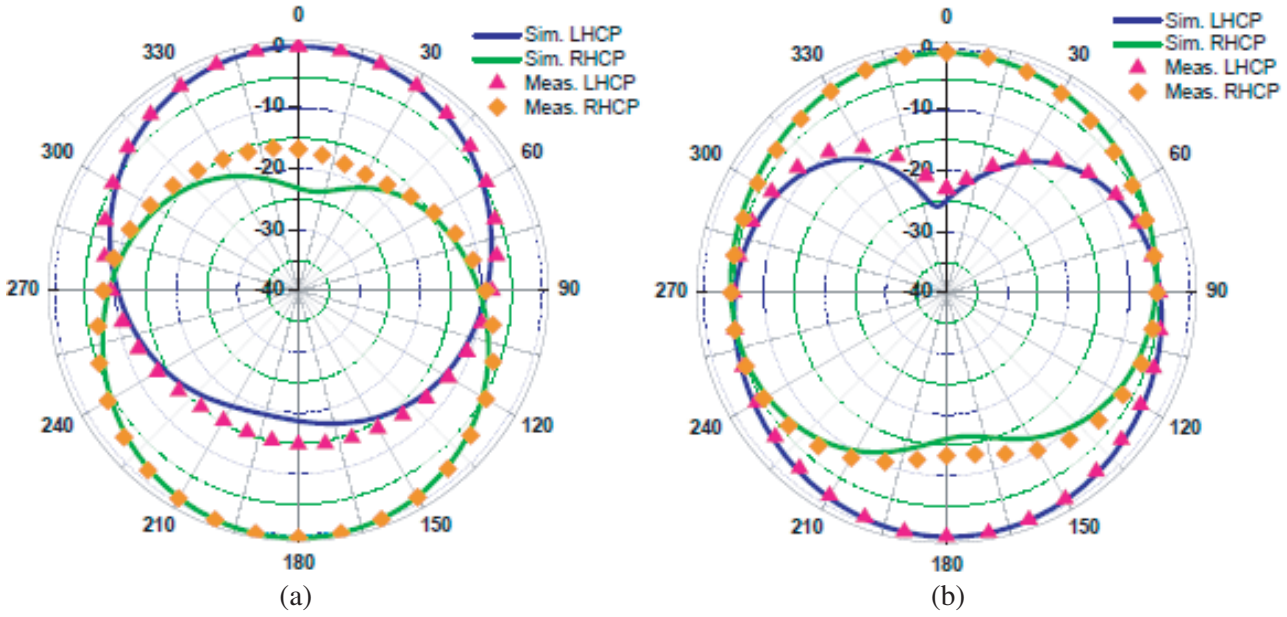

Figure 19. The numerical and measured CP radiation patterns (LHCP and RHCP) at (a) 4.28 GHz and (b) 6.3 GHz in YZ plane.

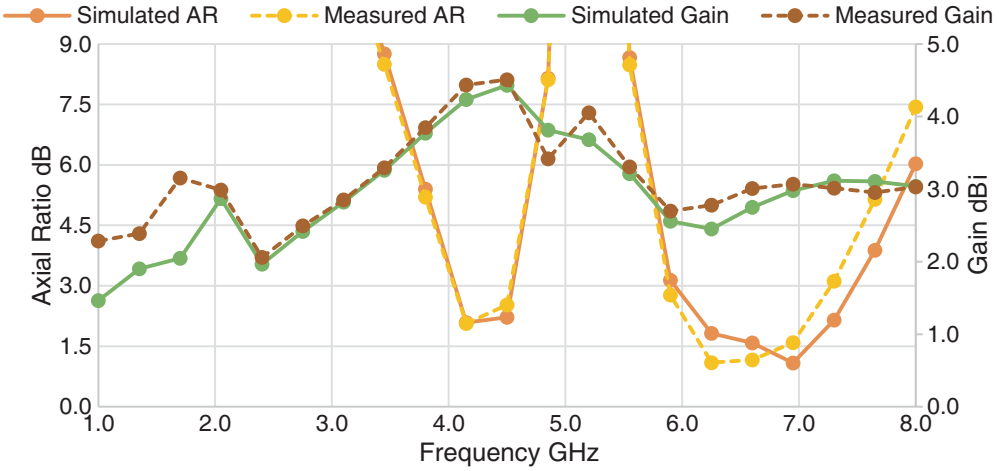

Figure 20. Simulated and measured axial ratio and antenna gain.

The variations of simulated and measured ARs and gains of the proposed antenna traces are plotted in Fig. 20 and found in agreement. The measured 3 dB ARBWs are 4.00–4.60 (4.28 GHz, 13.7%) and 6.07–7.13 (6.3 GHz, 16.6%). The measured values of peak gains at lower and upper-frequency bands are about 4.5 dBi and 3.1 dBi, respectively. In general, the gain in the upper band is larger than the lower band; however, in the offered design, it is less, which is probably due to the losses in the substrate material at high frequency. The variation of total and radiation efficiency values of 'antenna 3' with frequency are presented in Fig. 21. These efficiency values are comparable to other previously published designs mentioned in Table 2. The total and radiation efficiencies of the offered antenna are more than 90%.

Table 2 demonstrates the examination of the proposed antenna and different sorts of dual-band dual-sense CP antennas. The various antenna parameters such as dimension, gain, 3 dB ARBW, and −10 dB IBW of the presented antenna are compared with various antennas reported in the literature and

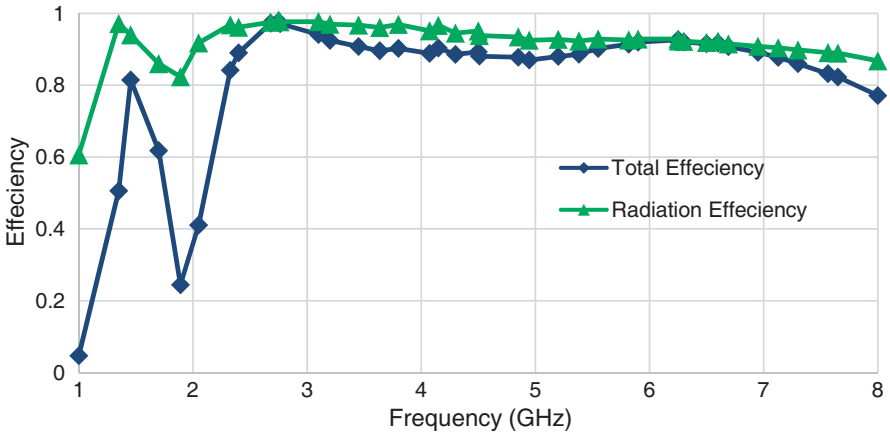

Figure 21. Variation of total and radiation efficiency of 'antenna 3' with frequency.

outlined in Table 2. It can be perceived from Table 2 that the proposed antenna provides the maximum IBW and wider CP bandwidth among the existing reported antennas with optimum dimensions of the antenna. The gain values in both bands are also improved.

Table 2. Comparison in performance of various dual frequency/band CP antennas.

Reference	−10 dB Reflection Coefficient Bandwidth (in GHz)		3 dB AR Bandwidth (in GHz)		Gain (in dBi)		Overall Dimension (mm × mm)	Efficiency (Radiation, Antenna)	
	Lower Band	Upper Band	Lower Band	Upper Band	Lower Band	Upper Band			
[5]	2.32–2.7	4.76–6	2.39–2.57	5.13–6.00	2.01–2.48	2.55–3.09	40 × 47	Not mentioned	
[6]	2.38–2.75	4.05–6.38	2.39–3	5.15–6.00	0.88–1.4	3.9–4.5	42.5 × 48	Not mentioned	
[9]	1.19–1.26	1.44–1.53	1.22–1.23	1.47–1.49	1.35	3.5	60 × 60	Not mentioned	
[12]	1.44–1.72	2.42–2.91	1.58–1.65	2.61–2.70	3.9–4.4	2.8–3.8	100 × 100	Not mentioned	
[13]	2.84–3.39	4.50–4.83	3.05–3.15	4.65–4.85	5.9	5.9	70 × 48	Not mentioned	
[14]	1.96–5.68		2.29–2.51	4.96–5.61	2.0	4.6	55 × 30	Not mentioned	
[23]	2.36–2.58	5.15–6.00	2.38–2.53	5.51–6.0	2.51	3.51	40 × 54	80% and 75% in lower band	72% and 68% in upper band
[24]	2.3–2.7	4.8–6.8	2.39–2.43	5.06–5.70	0.4–1.4	1.3–4.5	42 × 30	Not mentioned	
[25]	1.81–3.83		2.2–2.9	3.40–3.65	1.5–2.5	1.5–2.5	63 × 75	more than 90% in both the band	
[26]	2.3–3.7	3.1–3.8	2.37–2.57	-	1.0–1.6	1.1–1.57	40 × 40	more than 75% in both the band	
[27]	2.72–7.34		3.30–3.78	5.4–5.86	3.03	3.42	50 × 50	more than 90% in both the band	
proposed	**1.82–7.12**		**4.00–4.60**	**6.04–7.13**	**4.5**	**3.1**	64 × 32	more than 92% in both the band	

6. CONCLUSIONS

This paper presents the design and analysis of a dual-polarized antenna having wide bandwidth and reflects a dual-band CP behaviour to address the issue of alignment and orientation of communication systems. The design includes a modified circular shape printed dipole structure. To achieve this, elliptical slots of appropriate dimensions are etched in the ground and patch at appropriate positions supported by opening slots. The offered antenna has been fabricated on an FR-4 substrate after multiple computer simulations and examined experimentally. The measured resonance is at 2.72 GHz and 6.07 GHz with −10 dB impedance bandwidth 102.5% (2.36–7.34 GHz) along with 3 dB ARBWs 13.7% (4.00–4.60) in lower frequency bands and 16.6% (6.07–7.13 GHz) in upper frequency bands, respectively. At frequency 1.55 GHz, a linearly polarized behavior is also perceived which makes the offered antenna a dual-polarized antenna. The measured values of peak gains at lower and upper-frequency bands are 4.5 and 3.1 dBi, respectively. Moreover, the radiation patterns in the entire region of IBW are stable. This antenna may be useful for navigation and communication application in the S and C bands.

ACKNOWLEDGMENT

The authors would like to acknowledge the reviewers for their valuable comments. Authors also acknowledge the support of Dr. Sanjeev Yadav and Dr. Ashok Kumar, Government Mahila Engineering College, Ajmer, India for helping in the measurement of radiation patterns and Dr. Sarthak Singhal, MNIT Jaipur and Dr. Tejpal Jhajharia, Manipal University, Jaipur for their help in reply to comments of reviewers.

REFERENCES

1. Kumar, G. and K. P. Ray, *Broadband Microstrip Antenna*, Artech House, Boston, 2003.
2. Gao, S. S., Q. Luo, and F. Zhu, *Circularly Polarized Antennas*, Wiley-IEEE Press, UK, 2013.
3. Sharma, V., V. K. Saxena, K. B. Sharma, and D. Bhatnagar, "Radiation performance of circularly polarized broadband gap coupled elliptical patch antenna," *FREQUENZ Journal of RF-Engineering and Telecommunications*, Vol. 66, No. 3, 69–74, 2012.
4. Kumar, S., B. K. Kanaujia, M. K. Khandelwal, and A. K. Gautam, "Single-feed circularly polarized stacked patch antenna with small-frequency ratio for dual-band wireless applications," *International Journal of Microwave and Wireless Technologies*, Vol. 8, No. 8, 1207–1213, 2015.
5. Tan, M. T. and B. Z. Wang, "A dual-band circularly polarized planar monopole antenna for WLAN/Wi-Fi applications," *IEEE Antennas and Wireless Propagation Letters*, Vol. 15, 670–673, 2016.
6. Li, Q., Y. Wei, C. Ding, M. Tan, L. Zhang, X. Lei, G. Wu, Z. Wang, Z. Lu, and Y. Gong, "Dual-band circularly polarised planar monopole antenna for WLAN/Wi-Fi/Bluetooth/WiMAX applications," *IET Microwaves, Antennas & Propagation*, Vol. 12, No. 6, 972–976, 2018.
7. Kumar, S., R. K. Vishwakarm, R. Kumar, J. Anguera, and A. Andujar, "Slotted circularly polarized microstrip antenna for RFID application," *Radioengineering*, Vol. 26, No. 4, 1025–1032, December 2017.
8. Maddio, S., G. Pelosi, M. Righini, and S. Selleri, "A circularly polarized antenna for dual band operation at 2.45 GHz and 5.10 GHz," *Progress In Electromagnetics Research C*, Vol. 74, 1–8, 2017.
9. Bao, X. L. and M. J. Ammann, "Dual frequency circularly polarized patch antenna with compact size and small frequency ratio," *IEEE Transactions on Antennas and Propagation*, Vol. 55, No. 7, 2104–2107, 2007.
10. Wang, K., X. Liang, W. Zhu, J. Geng, J. Li, Z. Ding, and R. Jin, "A dual-wideband dual-polarized aperture-shared patch antenna with high isolation," *IEEE Antennas and Wireless Propagation Letters*, Vol. 17, No. 5, 735–738, 2018.
11. Bao, X. L. and M. J. Ammann, "Monofilar spiral slot antenna for dual-frequency dual-sense circular polarization," *IEEE Transactions on Antennas and Propagation*, Vol. 59, No. 8, 3061–3065, 2011.

12. Kandasamy, K., B. Majumder, J. Mukherjee, and K. P. Ray, "Dual-band circularly polarized split ring resonators loaded square slot antenna," *IEEE Transactions on Antennas and Propagation*, Vol. 64, No. 8, 3640–3645, 2016.
13. Bhattacharjee, S., S. Maity, S. R. B. Chaudhuri, and M. Mitra, "A compact dual-band dual-polarized omnidirectional antenna for on-body applications," *IEEE Transactions on Antennas and Propagation*, Vol. 67, No. 8, 5044–5053, 2019.
14. Xu, R., J. Li, and G. Yang, "A novel dual-band dual-sense circularly polarized antenna based on simple printed dipole structure," *IEEE International Symposium on Antennas and Propagation & USNC/URSI National Radio Science Meeting*, 2017.
15. Bhattacharjee, S., M. Madiya, M. Mitra, and S. R. B. Chaudhuri, "Dual band-dual polarized planar inverted F-antenna for MBAN applications," *International Journal of Microwave and Wireless Technologies*, Vol. 11, No. 1, 76-861–11, 2019.
16. Midya, M., S. Bhattacharjee, G. K. Das, and M. Mitra, "Dual-band dual-polarized compact planar monopole antenna for wide axial ratio bandwidth application," *International Journal of RF and Microwave Computer-Aided Engineering*, Vol. 30, No. 5, 1–10, 2020.
17. Agrawall, N. P., G. Kumar, and K. P. Ray, "Wide-band planar monopole antennas," *IEEE Transactions on Antennas and Propagation*, Vol. 46, No. 2, 294, 1998.
18. EM Simulation Software — CST Studio Suite, 2017.
19. Jhajharia, T., V. Tiwari, D. Bhatnagar, D. Yadav, and S. Rawat, "A dual-band CP dual-orthogonal arms monopole antenna with slanting edge DGS for C-band wireless applications," *AEU — International Journal of Electronics and Communications*, Vol. 84, 251–257, 2018.
20. Jhajharia, T., V. Tiwari, and D. Bhatnagar, "Polarisation reconfigurable dual-band circularly polarised patch antenna with defected ground plane for C-band wireless applications," *IET Microwaves, Antennas & Propagation*, Vol. 13, No. 14, 2551–2558, 2019.
21. https://www.keysight.com/en/pdx-x201916-pn-N5234A/pna-l-microwave-network-analyzer-435-ghz?cc=IN&lc=eng, 2019.
22. IEEE Standard Test Procedures for Antennas, *ANSI/IEEE Std*, 149-1979, 1979.
23. Niyamanon, S., R. Senathong, and C. Phongcharoenpanich, "Dual frequency circularly polarized truncated square aperture patch antenna with slant strip and L-shaped slot for WLAN applications," *International Journal of Antennas and Propagation*, Vol. 2018, Article ID 7684742, 11 pages, 2018.
24. Liang, W., Y. Jiao, Y. Luan, and C. Tian, "A dual-band circularly polarized complementary antenna," *IEEE Antennas and Wireless Propagation Letters*, Vol. 14, 1153–1156, 2015.
25. Saini, R. K., S. Dwari, and M. K. Mandal, "CPW fed dual-band dual-sense circularly polarized monopole antenna," *IEEE Antennas and Wireless Propagation Letters*, Vol. 16, 2497–2500, 2017.
26. Shi, S., W. P. Ding, and K. Luo, "A monopole antenna with dual-band reconfigurable circular polarization," *Progress In Electromagnetics Research C*, Vol. 55, 35–42, 2014.
27. Midya, M., S. Bhattacharjee, and M. Mitra, "CPW-fed dual-band dual-sense circularly polarized antenna for WiMAX application," *Progress In Electromagnetics Research Letters*, Vol. 81, 113–120, 2019.